

Additive Manufacturing of 17-4 PH Stainless Steel: Post-processing Heat Treatment to Achieve Uniform Reproducible Microstructure

SUDHA CHERUVATHUR,¹ ERIC A. LASS,^{1,2} and CARELYN E. CAMPBELL¹

1.—Materials Science and Engineering Division, Materials Measurement Laboratory, National Institute of Standards and Technology, Gaithersburg, MD 20899, USA. 2.—e-mail: eric.lass@nist.gov

17-4 precipitation hardenable (PH) stainless steel is a useful material when a combination of high strength and good corrosion resistance up to about 315°C is required. In the wrought form, this steel has a fully martensitic structure that can be strengthened by precipitation of fine Cu-rich face-centered cubic phase upon aging. When fabricated via additive manufacturing (AM), specifically laser powder-bed fusion, 17-4 PH steel exhibits a dendritic structure containing a substantial fraction of nearly 50% of retained austenite along with body centered cubic/martensite and fine niobium carbides preferentially aligned along interdendritic boundaries. The effect of post-build thermal processing on the material microstructure is studied in comparison to that of conventionally produced wrought 17-4 PH with the intention of creating a more uniform, fully martensitic microstructure. The recommended stress relief heat treatment currently employed in industry for post-processing of AM 17-4 PH steel is found to have little effect on the as-built dendritic microstructure. It is found that, by implementing the recommended homogenization heat treatment regimen of Aerospace Materials Specification 5355 for CB7Cu-1, a casting alloy analog to 17-4 PH, the dendritic solidification structure is eliminated, resulting in a microstructure containing about 90% martensite with 10% retained austenite.

INTRODUCTION

17-4 PH is a martensitic precipitation hardenable stainless steel having high strength and good corrosion resistance, suitable for applications involving thermal exposure up to 315°C. When fabricated through conventional routes, the alloy has a fully martensitic structure (with the exception of a small fraction of body centered cubic (BCC) δ -ferrite) that has poor ductility and susceptibility for embrittlement and stress corrosion cracking.¹ Hence, most of the earlier studies^{2–6} focused on improving the mechanical properties of 17-4 steel through aging treatment in the low temperature (<Ac1; the temperature at which face-centered cubic (FCC)/austenite phase begins to form in the steel) regime. Based on these investigations, a fairly good understanding has been obtained of various stages of evolution of microstructure in

‘conventionally’ produced 17-4 steel upon annealing in the temperature and time ranges of 400°C to 650°C and 5 min to 5000 h, respectively.

The renewed interest in ‘customized’ low volume products and cost-effective environmental friendly manufacturing technology for specialized applications has shifted the focus from ‘conventional’ to ‘additive’ manufacturing (AM) of various materials, including 17-4 steel. AM technology offers a novel processing route for fabricating near-net-shape parts with complex geometries that are difficult or impossible to create via other fabrication methods.^{7,8} However, processing conditions can vary greatly from those produced via conventional methods, resulting in nonuniform, highly anisotropic, material properties.^{9,10} This exposed the inadequacy of extending the previously acquired knowledge on microstructural evolution in 17-4 steel (and other materials) to those produced via the AM route.

Existing literature on AM 17-4 steel reveal strong dependence of material microstructure and phase constitution on process parameters, particularly the presence of a significant fraction of retained austenite. Several reasons have been cited in the literature for the formation of retained austenite^{11–15} in an additively manufactured steel: (1) presence of strain at high-angle grain boundaries which suppress the transformation of austenite to martensite, (2) relatively higher dislocation density, (3) supersaturation of γ with the corresponding phase stabilizing elements, (4) smaller grain sizes and interdendritic spacing and (5) powder manufacturing environment. Of these, the powder atomization and AM build chamber environments (Ar or N₂ gas) have demonstrated significant effects on the amount of retained austenite in AM 17-4 steel.^{11–14} Murr et al. reported^{12,13} that 17-4 PH steel fabricated using selective laser melting method in Ar/Ar (powder atomization/AM environment), Ar/N₂ and N₂/Ar atmosphere had a martensitic, α' , structure, whereas in N₂/N₂ it was predominantly gamma (FCC/austenite) with 15% of α' . In addition, the as-built parts showed a strong difference in texture components parallel and perpendicular to the build direction. In a similar study,¹⁴ FCC was the predominant phase in the part built in a N₂ environment irrespective of whether the powder was atomized in Ar or N₂. The FCC phase of a specific composition, present in the martensite lath boundaries, was observed to be difficult to harden by standard aging heat treatments recommended for 17-4 steel. Upon exposure to temperatures > 788°C, substantial transformation of FCC to α' phase was observed, opening up interesting possibilities to tailor the microstructure of AM 17-4 steel to exhibit a transformation-induced plasticity (TRIP) effect.¹⁵

With this as the motivation, in the present work the authors have tried to manipulate 17-4 steel produced via AM by tailoring the post-processing heat treatment to create a reproducible microstructure with known, predictable properties comparable to conventional counterparts.

EXPERIMENTAL DETAILS

Table I shows the chemical composition of pre-alloyed and rapidly solidified 17-4 steel powder used in the present study. The powders were atomized using nitrogen gas and the fraction of particles > 53 μm was found to be 4.2% via sieve analysis. An electro optical systems (EOS)¹⁶ M270 Laser powder-bed fusion,¹⁷ additive manufacturing instrument was used to fabricate the test specimens. The “skin & core” building style described by EOS¹⁸ was used for increased building speed. A Nd:YAG laser operating at a power of 195 W was scanned at a speed of 1000 mm/s on a pre-laid powder bed to form a striped scan pattern of a 0.1-mm stripe in raster separation. Laser parameters were optimized to achieve a layer thickness of 20 μm . Volume build and energy densities were maintained at 2 mm³/s and 97.5 J/mm², respectively. Nitrogen was used as the purging gas. Test blocks with dimensions of 1.1 cm by 1.1 cm by 0.5 cm were built on a build plate (made of 1045 steel) 25 mm in height. Post-build, test blocks were cut and separated from the build plate using electrical discharge machining without a stress relieving heat treatment.

For microstructural characterization, multiple specimens were extracted from the same as-built test blocks both parallel (cross-section) and perpendicular (z direction) to the build direction. To study the effect of thermal exposure on microstructure and phase evolution, the as-built specimens were heat-treated after encapsulating in quartz ampules under Ar atmosphere. The temperatures and times of heat treatment were chosen as 650°C and 1050°C for 1 h and 1150°C for 2 h to adhere to the EOS technical specification,¹⁸ wrought solutionizing heat treatment, condition A,¹⁹ and AMS 5355 homogenizing heat treatment,²⁰ respectively. For comparison, wrought 17-4 steel (composition given in Table II) was also examined in the as-received and solution-treated conditions. Carbon content in the wrought steel was determined as 0.02 (mass fraction times 100) as per ASTM E1019. To facilitate

Table I. Chemical composition (mass fraction times 100) of 17-4 steel powders used in the present study (no uncertainty was provided by the manufacturer)

Cr	Ni	Cu	Mn	Si	Mo	Nb	C	S	P	Fe
15.4	4.3	4.0	0.6	0.7	0.1	0.27	0.05	0.01	0.02	Balance

Table II. Chemical composition (mass fraction times 100) of wrought 17-4 steel based on EDS analysis (no uncertainty was provided by third-party testing laboratory)

Cr	Ni	Cu	Mn	Si	Mo	Nb	Fe
16.51	4.33	4.83	0.72	0.47	0.15	0.45	Balance

Table III. Labels used for identifying the specimens

Sample details	Label	Hardness (VHN)
AM—as built	AM-AB	258 ± 8
AM—EOS stress-relieving heat treatment	AM-SR	312 ± 17
AM—wrought solutionizing heat treatment	AM-S	318 ± 24
AM—AMS 5355 homogenizing heat treatment	AM-H	288 ± 32
Wrought—as-received	W-AR	322 ± 10
Wrought—solution-treated condition	W-S	299 ± 11

further discussion, various specimens are labeled as given in Table III. Temperature fluctuation during heat treatment was maintained to be $\pm 5^\circ\text{C}$. After thermal exposure, the specimens were quenched in agitated brine solution without breaking the quartz tubes to achieve a cooling rate similar to air cooling.

All samples were polished by standard metallography procedures and etched using Swede's etchant (50 mL H_2O + 5 mL HCl + 5 mL HNO_3 + 6 g FeCl_3) to reveal the microstructure. Microstructural observations were carried out using both optical (Leica DMIRM equipped with DC500 CCD camera) and scanning electron microscopy (SEM; JEOL JSM-7100FT FESEM). Microchemical analysis was performed using the JEOL SEM attached to a silicon drift detector for energy dispersive spectroscopy (EDS) analysis at an operating voltage and current of 15 kV and 1.5 nA, respectively. Hardness was measured on polished specimen surfaces at a magnification of $\times 50$ using a Vicker's microhardness tester (Leica VMHT Auto) after applying a load of 100 g for 10 s. The reported hardness values are the average of ten measurements from randomly chosen locations. Phase identification was conducted using a Philips x-ray diffractometer using $\text{Cu K}\alpha$ radiation at an operating voltage and current of 45 kV and 40 mA, respectively. x-ray diffraction patterns were obtained within a 2θ range of 20° to 100° at a step size of 0.05° with the counting time of 1 s per step. Because of the very low tetragonality of the martensite phase in the 17-4 steel, it was indistinguishable from the BCC ferrite phase in XRD; and both phases are referred to simply as BCC/martensite.

Non-equilibrium solidification simulations and equilibrium phase diagram calculations were performed using the Thermo-Calc software²¹ integrated with TCFE6 database.²² A nominal composition of Fe-15.4Cr-4.3Ni-4.0Cu-0.27Nb-0.05C (in mass fraction times 100) for the alloy was assumed. Scheil calculations were performed for a step size of 1°C up to a remnant liquid mole fraction of ≈ 0.01 , ignoring the back diffusion of carbon.

RESULTS AND DISCUSSION

Microstructure of Wrought 17-4 PH Steel

Figure 1a shows the typical martensitic microstructure of as-received wrought 17-4 steel having a hardness of 322 ± 10 Vicker's hardness

number (VHN). δ -ferrite stringers are observed likely aligned along the rolling direction (formed during initial solidification). The x-ray diffraction (XRD) pattern has Bragg reflections corresponding to only BCC/martensite (Fig. 1b). After subjecting to condition A heat treatment, the α' lath structure is retained (Fig. 1c and d), and the material has a hardness of 299 ± 11 VHN. Examining the microstructure at a higher magnification reveals the presence of fine ($\leq 1 \mu\text{m}$) precipitates throughout the matrix (Fig. 1e). Based on x-ray mapping (Fig. 1f), these precipitates are presumed to be Nb-rich carbides.

Change in the Microstructure of 17-4 Steel Due to Additive Manufacturing

The optical micrograph (Fig. 2a) shows the microstructure of as-built AM 17-4 steel perpendicular to the build direction. Laser tracks are visible from the micrograph. For the given energy density of the laser, the maximum width of a melted region in a single track appear to be $\approx 100 \mu\text{m}$. Observing the microstructure along the build direction (Fig. 2b) reveals the overlapping hemispherical melt pools created by the laser with the individual melt pool heights ranging from $20 \mu\text{m}$ to $50 \mu\text{m}$. If the melt pools are assumed to be hemispherical, this suggests as much as 50% of the previous layer is remelted upon the addition of a subsequent layer. The as-built steel has a hardness of only 258 ± 8 VHN, lower than its wrought counterpart. Closer examination of the microstructure within individual melt pools (Fig. 2c) reveals a dendritic-cellular solidification structure. The dendrites are oriented predominantly along the build direction, indicating that the general direction of heat flow during solidification is through the build plate; though they often occur at some angle off the build direction axis (region marked by an arrow in Fig. 2c), indicating that other effects, such as the direction of the laser scan, play a role in the local heat flow. Between the primary dendrites/cells, white nanoscale precipitates are observed (identified below as Nb-rich carbides). Primary grains spanned several melt pool layer thicknesses. Primary and secondary dendrite spacings of the order of only $\approx 0.3 \mu\text{m}$ and (100–200) nm, respectively, are observed in the as-built material. These fine dendrite spacings, effectively subgrains isolated by the interdendritic

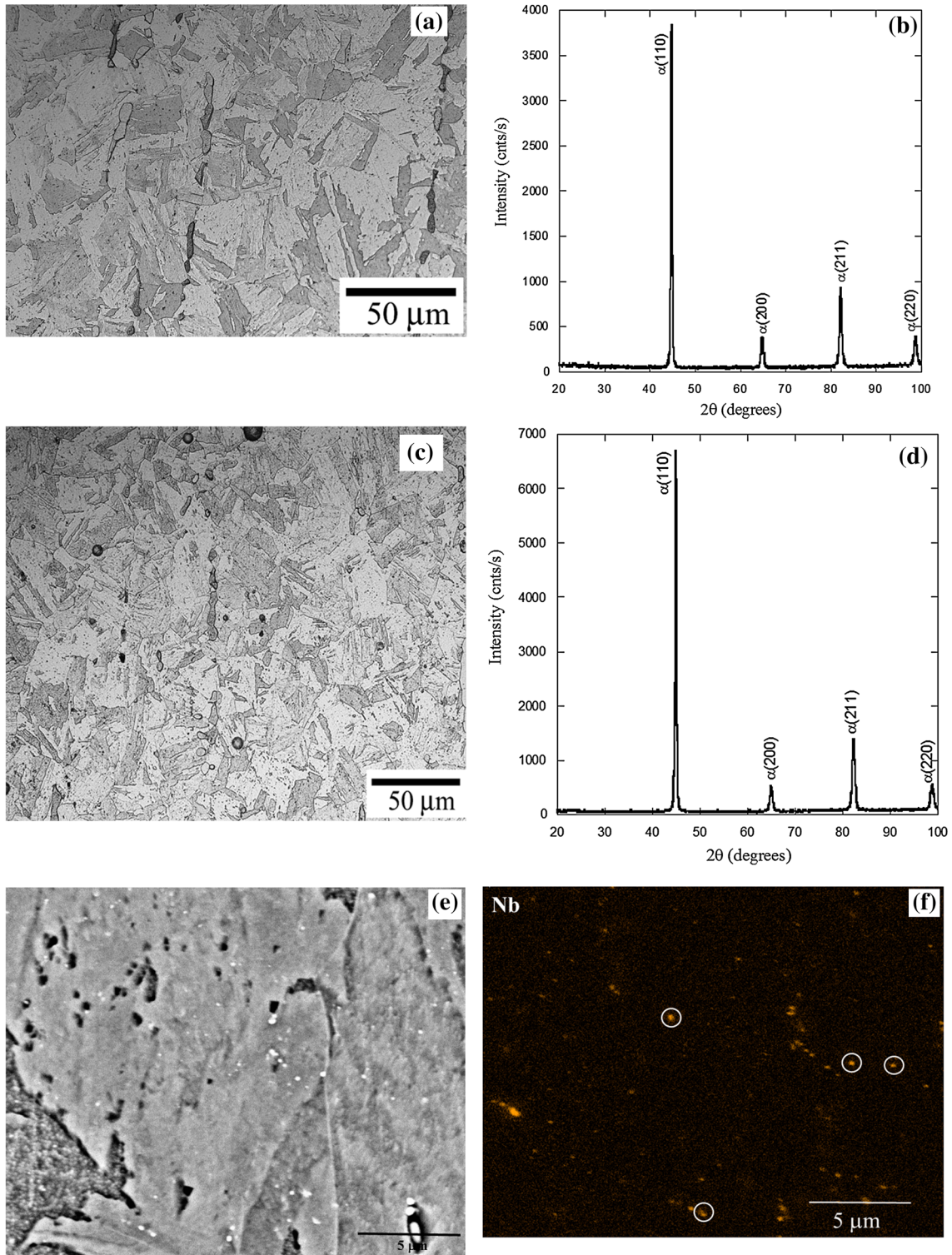


Fig. 1. (a, b) Optical micrograph and XRD pattern showing fully BCC/martensite structure of the W-AR steel. (c, d) Optical micrograph and XRD pattern and (e, f) SE image and x-ray map obtained from the W-S steel revealing fully BCC/martensite structure with fine ($<1 \mu\text{m}$) niobium carbides (some of the carbides are highlighted).

regions, are a result of the high solidification rates experienced during AM.²³ Compared to the microstructure of wrought steel (Fig. 1a), these subgrains are extremely fine in an AM steel. No

macro-segregation is observed across the melt puddles. The as-built test specimen is essentially free of defects, although the top surface has the occasional presence of oxide inclusions and porosity.

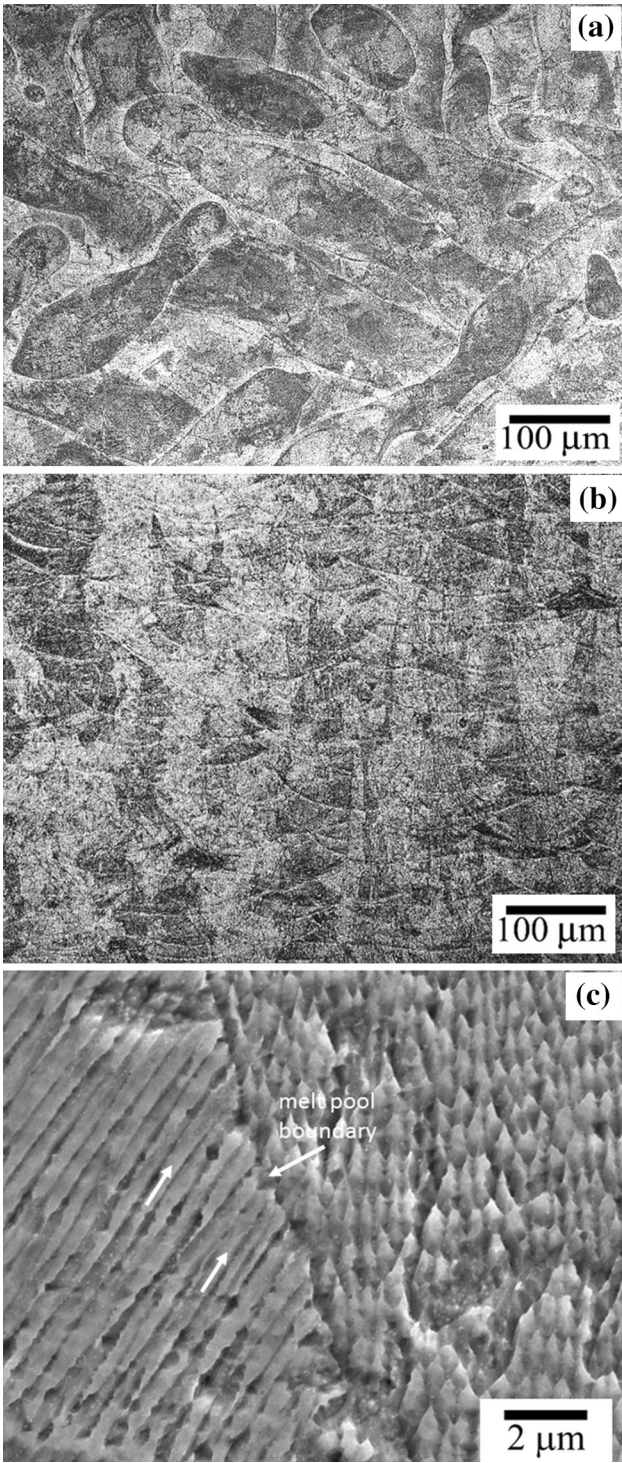
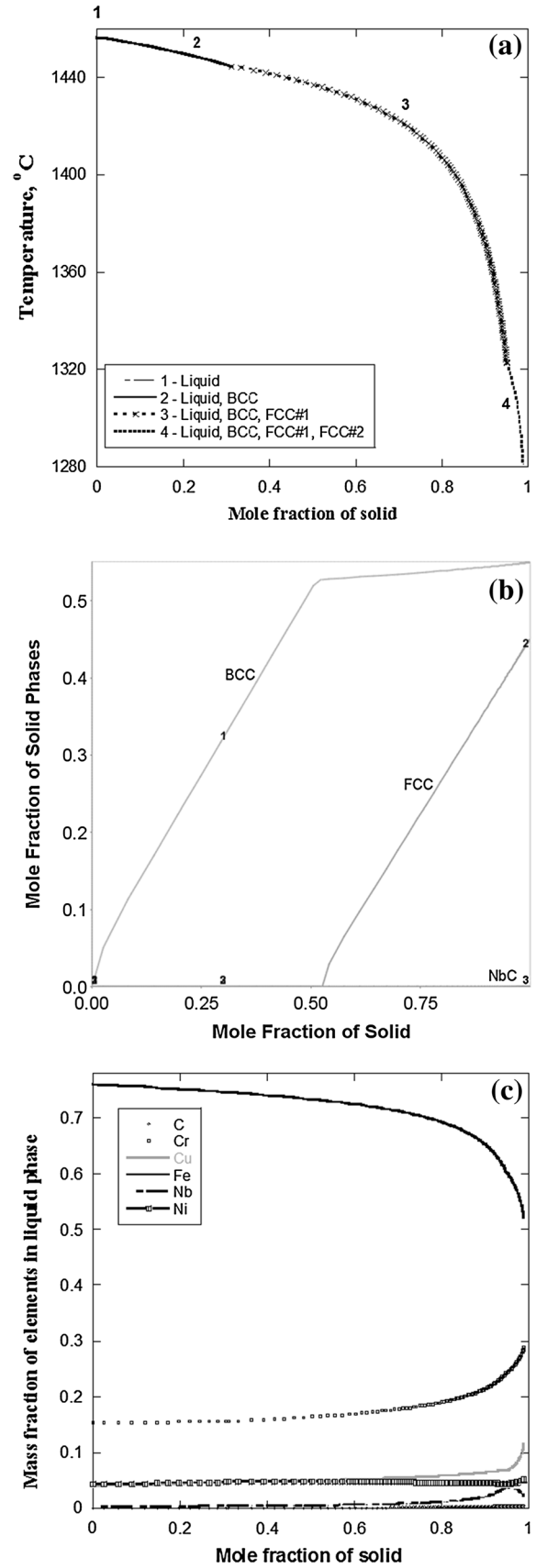


Fig. 2. Optical micrographs of the AM-AB 17-4 steel showing the microstructure (a) perpendicular and (b) parallel to the build direction, and (c) SE image revealing the dendritic-cellular solidification structure.

Fig. 3. Scheil–Gulliver non-equilibrium solidification simulation revealing (a) the solid phases that evolve from the liquid with decreasing temperature, (b) the mole fraction of individual solid phases and (c) change in the mass fraction of each element in the liquid phase as the solidification front proceeds.



The microstructure and phase constituents of an alloy obtained via an additive route may be completely different from that obtained through regular fabrication procedures. Conventionally cast alloys have comparatively slower cooling rates, and wrought materials are thermo-mechanically processed after casting to break up the solidification structure and create a more homogeneous material. The high cooling rates (10^3 °C/s to 10^5 °C/s) in AM²³ may result in more prominent microsegregation features. Hence, during AM, as a first approximation, it is reasonable to assume negligible diffusion in the solid state, in which case the solidification and microsegregation behavior can be assessed using Scheil–Gulliver model.

Figure 3a shows the variation in the mole fraction of solid with temperature as the alloy is cooled from the liquid phase region. The first phase to form from the liquid is BCC/ferrite followed by BCC + FCC/austenite. Towards the end of solidification niobium rich MC carbide phase (FCC#2) is observed to form from the liquid. Figure 3b reveals that, when solidification is roughly 50% complete, the FCC phase becomes the primary solidification phase, and as solidification reaches completion, there are approximately equal fractions of BCC and FCC phases in addition to <0.01% of NbC. When the change in weight fraction of different elements is plotted against the mole fraction of the solid (Fig. 3c), elements like Cr, Cu, Nb and C are found to partition to the liquid, and the last liquid to solidify contains mass fractions of nearly 30% Cr, 10% Cu and 4% Nb. Based on these results, the microstructure and microchemistry of as-built AM 17-4 steel is expected to be as follows: cell/dendrite cores of BCC phase, with outer dendrite shells of primarily FCC phase with some BCC. The last to solidify interdendritic regions contain the NbC phase. Assumption of partial equilibrium does not influence the microsegregation behavior. This is in accordance with the observation of Chen and Sundman²⁴ that, in steels with ferrite as the primary solidification phase, assumption of carbon back diffusion may not improve the calculation since the rest of the substitutional elements may also have reasonably fast diffusivity in ferrite.

An XRD pattern (Fig. 4) obtained from an AM-AB specimen parallel to the build direction confirms the presence of both FCC and BCC phases as predicted from the simulations. Using the integrated intensity of the peaks, the relative volume fraction of the phases are calculated as roughly 50% FCC/austenite and 50% BCC/martensite. The presence of such a high volume fraction of FCC phase explains the relatively lower hardness obtained for as-built material. Figure 5a shows a high magnification secondary electron (SE) image obtained from AM-AB steel. x-ray maps for Fe, Cr, Nb and C (Fig. 5b–e) from the region marked in Fig. 5a confirm the presence of fine Nb carbides, as predicted by the

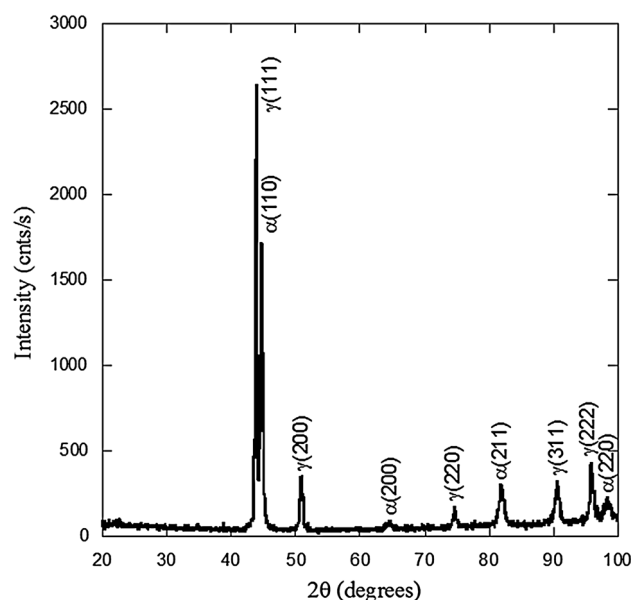


Fig. 4. XRD pattern obtained from the AM-AB 17-4 steel parallel to the build direction.

Scheil simulation. Fe and Cr are relatively enriched in the dendrite cores (Fig. 5b and c) where the simulations predict BCC phase formation.

The above detailed examination confirms the presence of retained austenite in as-built AM 17-4 steel. Out of various possibilities, the formation of retained austenite appears to be highly likely due to the absorption of nitrogen, an austenite stabilizer, from both powder processing and AM environments, resulting in a decreased martensite transition start temperature, M_s . Another reason could be the extremely fine subgrain sizes obtained during AM that again lower the M_s temperature and suppress the martensitic transformation.²⁵ For AISI 420 steel, the M_s temperature corresponding to a grain size of $100\ \mu\text{m}$ is 115°C . Following laser surface melting, the grain size reduced to $2.7\ \mu\text{m}$ and M_s temperature shows a corresponding decrease to 20°C .²⁶ A similar behavior can also be expected for AM 17-4 steel. Further, microsegregation during additive manufacturing may lead to the FCC phase enriched in austenite stabilizers, suppressing the martensite transition compositionally. Similar observations have been made for maraging steels.²⁷

A two-phase structure consisting of martensite and retained austenite may have both detrimental and beneficial effects on the mechanical and corrosion properties of the alloy. The nature and extent of this effect is dictated by the stability of the FCC phase which is linked to its chemistry. Some retained austenite-containing steels exhibit large elongation to failure due to strain-induced transformation of $\gamma \rightarrow \alpha'$.¹⁵ Yet, having a softer constituent

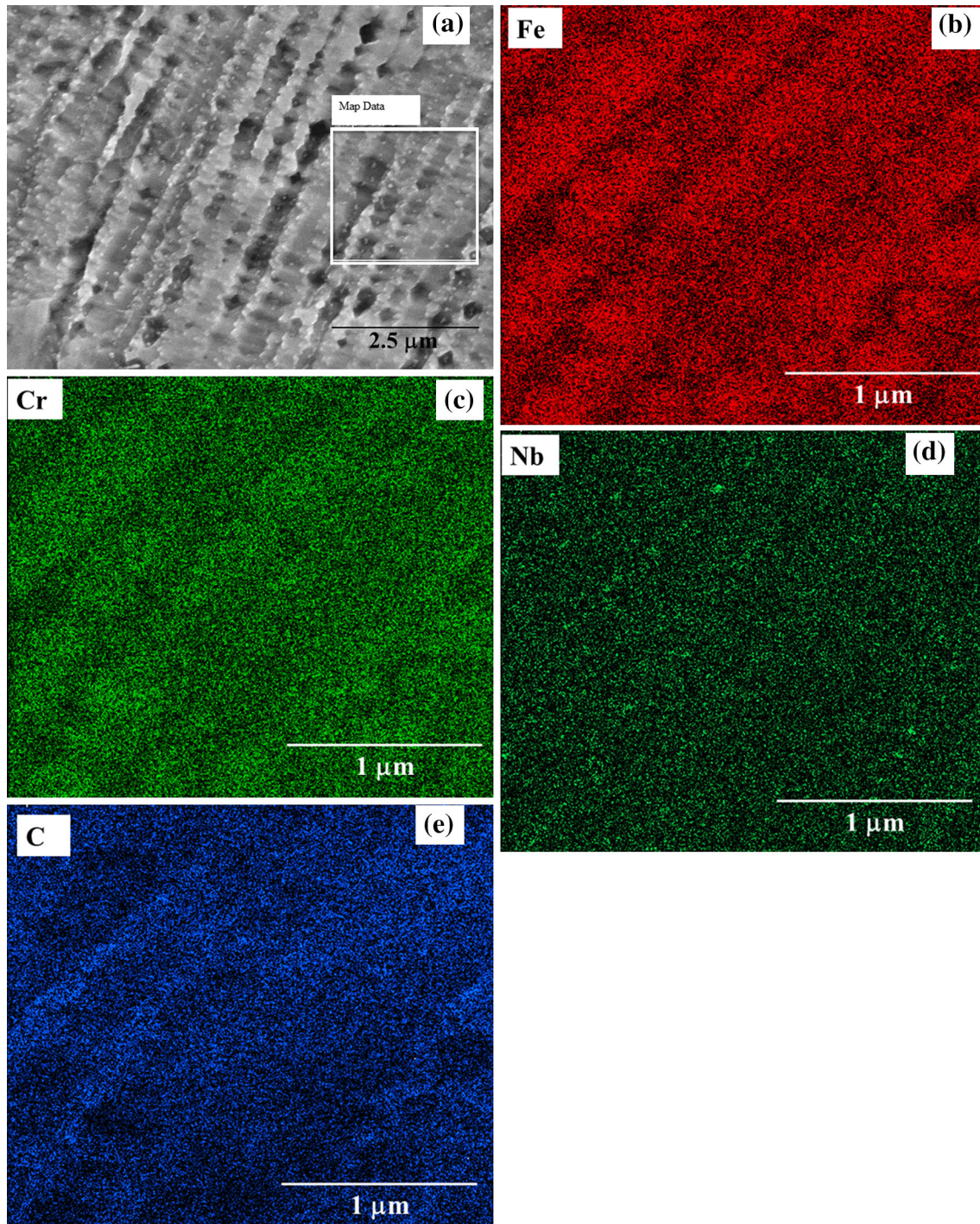


Fig. 5. SE image showing the presence of fine precipitates in inter-dendritic regions and x-ray map acquired from the highlighted region in (a) giving evidence for the enrichment of (b) Fe and (c) Cr in dendrite cores and (d) Nb and (e) C in inter-dendritic regions in AM-AB 17-4 steel.

like austenite in the matrix is harmful for the wear resistance of an alloy. In addition, the volume change associated with the phase transformation increases the propensity for cracking.²⁸ In the present study, Scheil simulations predict, and x-ray mapping illustrates, the presence of compositionally inhomogeneous, cored microstructures. In addition, the microsegregation can lead to the

formation of unexpected phases and/or inhomogeneous, unreliable properties. These compositional and microstructural inhomogeneities must be eliminated in AM 17-4 steel components to avoid the detrimental effects they introduce.

Several methods have been suggested in the literature to reduce the volume fraction of metastable retained austenite, but they lead to

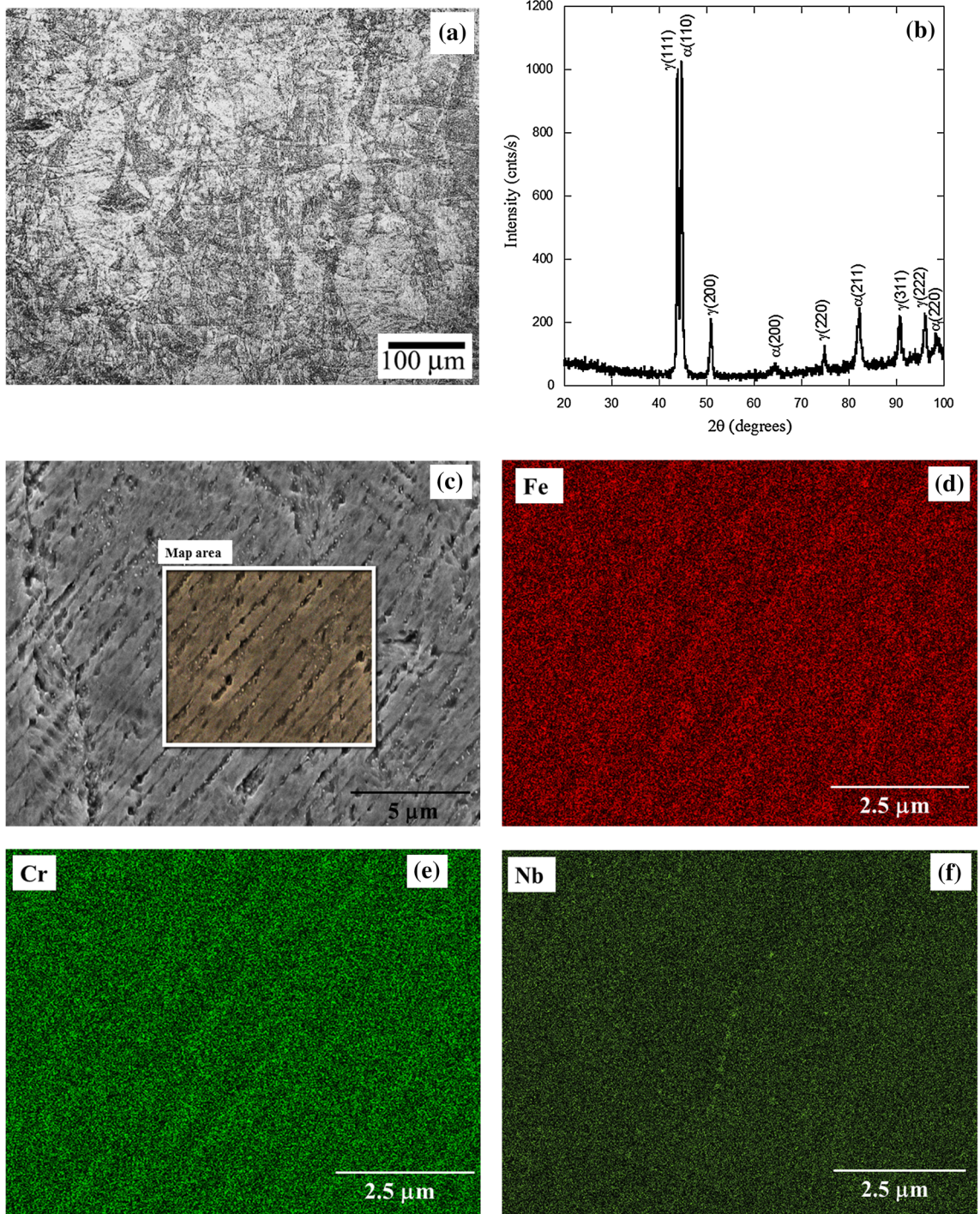


Fig. 6. (a) Optical micrograph. (b) XRD pattern. (c) SE image. (d-f) x-ray maps for Fe, Cr and Nb respectively obtained parallel to the build direction from AM-SR steel.

substantial modification of the secondary phases. Multiple tempering cycle heat treatments¹⁴ create extensively softer material due to coarsening of carbides, whereas cryogenic treatments²⁹ employing dry ice as the coolant modify the amount and population density of secondary carbides that evolve

during subsequent tempering cycles. Since thermo-mechanical processing of as-built structures defeat much of the purpose of choosing the AM route, the authors have employed various 'industrially accepted' thermal treatment schedules to investigate their effect on the microstructure.

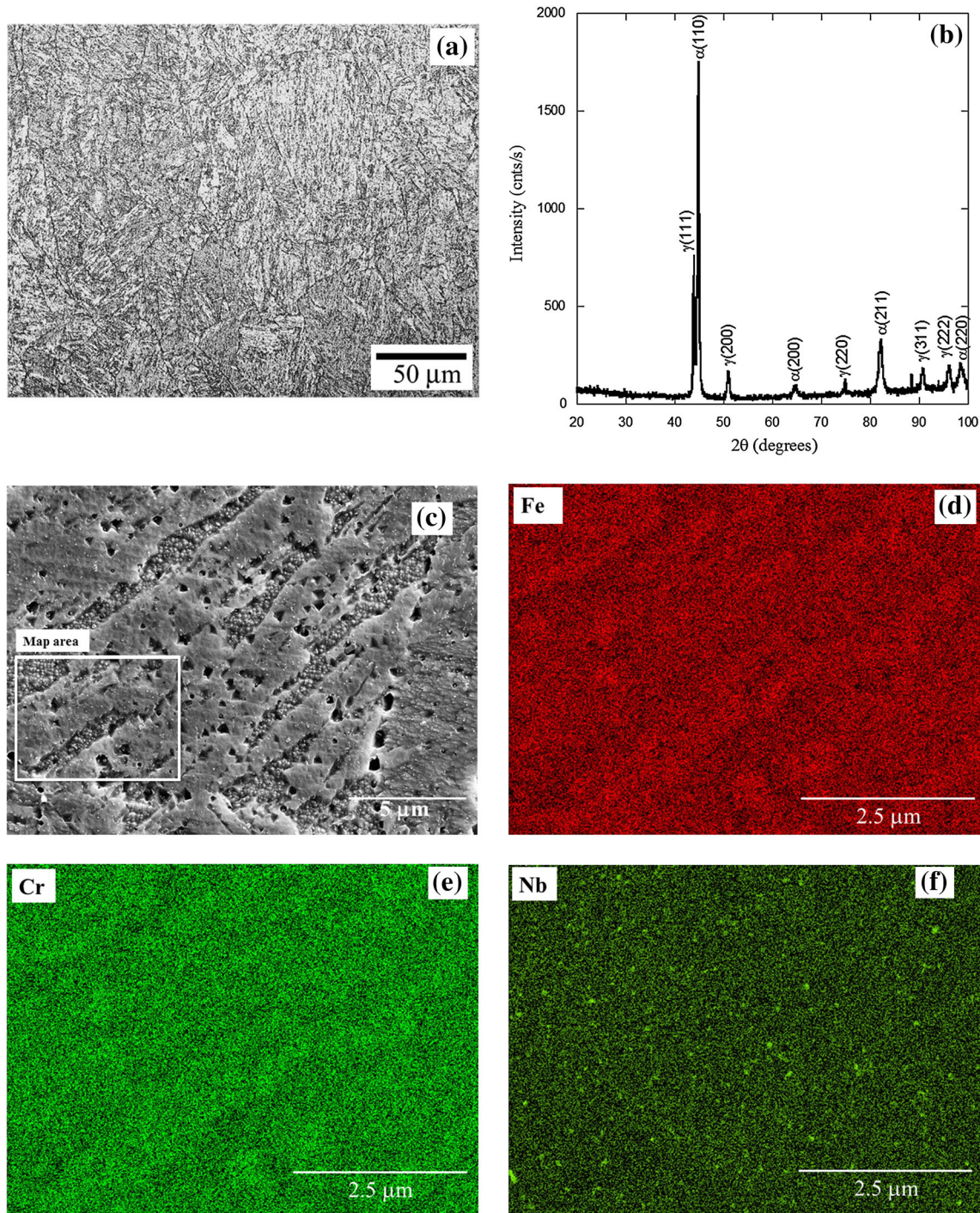


Fig. 7. (a) Optical micrograph. (b) XRD pattern. (c) SE image. (d–f) x-ray maps for Fe, Cr and Nb respectively obtained parallel to the build direction from AM-S steel.

Effect of Heat Treatment on the Microstructure of AM 17-4 Steel

An optical micrograph, XRD pattern, SE image and x-ray maps (for Fe, Cr and Nb) obtained parallel to the build direction for AM-SR steel are given as Fig. 6a–f, respectively. The EOS heat treatment produces very little change in the dendritic/cellular solidification microstructure. The melt pool traces

are still visible in the material as shown in Fig. 6a. XRD analysis (Fig. 6b) shows a relatively (in comparison with Fig. 4) small decrease in the volume fraction of FCC phase. As in the case of AM-AB steel (Fig. 5), microsegregation of Nb and C to interdendritic regions is observed. EOS stress relieving heat treatment increases the hardness to 312 ± 17 VHN, near that of wrought steel, despite retaining a

significant fraction of FCC/austenite. This increase in hardness is possibly due to several factors, including the small decrease in retained austenite (and increase in BCC/martensite), or the precipitation of Cu-rich secondary phases within α' laths as observed during the aging of wrought steel beyond 580°C.⁴

Figure 7a and b shows the microstructure and XRD pattern of AM-S steel. Compared to the stress-relieving heat treatment, the microstructure appears to be predominantly a martensitic structure with no trace of the melt pools. Based on XRD analysis, the dominant phase in the steel is confirmed to be martensite with the amount of retained austenite now reduced to approximately 15% to 20%. Based on the analysis of the microstructure at high magnification (Fig. 7c) and acquired x-ray maps (Fig. 7d–f), microsegregation is still confirmed to be present along former dendrite directions. Compared to the AM-AB and AM-SR specimens, niobium carbides have coarsened. These results indicate that the annealing temperature and hold time are insufficient to dissolve the carbide phases and homogenize the fine variation in the microchemistry. This heat treatment results in a hardness (318 ± 24 VHN) roughly equal to that of wrought steel, which can be attributed to the predominance of martensite in the microstructure and reduction in the amount of retained austenite compared to AM-AB and AM-SR steels.

Stability of Phases at High Temperature Under Equilibrium Conditions

Figure 8a and b shows the isopleth sections of the phase diagram as a function of carbon and niobium concentrations, respectively. According to Fig. 8a, for the given alloy composition (marked by a black vertical line), BCC-ferrite + FCC-Austenite (FCC#1) + Cu-rich FCC (FCC#2) + MC + $M_{23}C_6$ are the stable phases at a temperature of 650°C. At a higher temperature of 1050°C, only FCC-Austenite + MC type niobium carbides are stable. As observed in the case of AM-AB steel, if there is a local increase in the concentration of niobium due to microsegregation, the stability of the phases at 650°C is shifted from BCC + FCC#1 + FCC#2 + MC + $M_{23}C_6$ to BCC + FCC#1 + FCC#2 + MC (Fig. 8b). From the isopleth sections, it is also evident that the employed heat treatments are below the MC carbide solvus (> 1250°C), explaining their coarsening after wrought solutionizing heat treatment (Fig. 7f). For the given alloy composition, both NbC and $M_{23}C_6$ are predicted to form. While NbC is presumed to be present based on x-ray mapping, $M_{23}C_6$ is not found possibly due to the low volume fraction expected. Even though FCC phase separation into Fe- and Cu-rich phases is expected, the Cu-rich phase is not detected in XRD patterns, likely due to their low mass fraction and nanoscale size. The Cu-rich phase has been reported to be fine

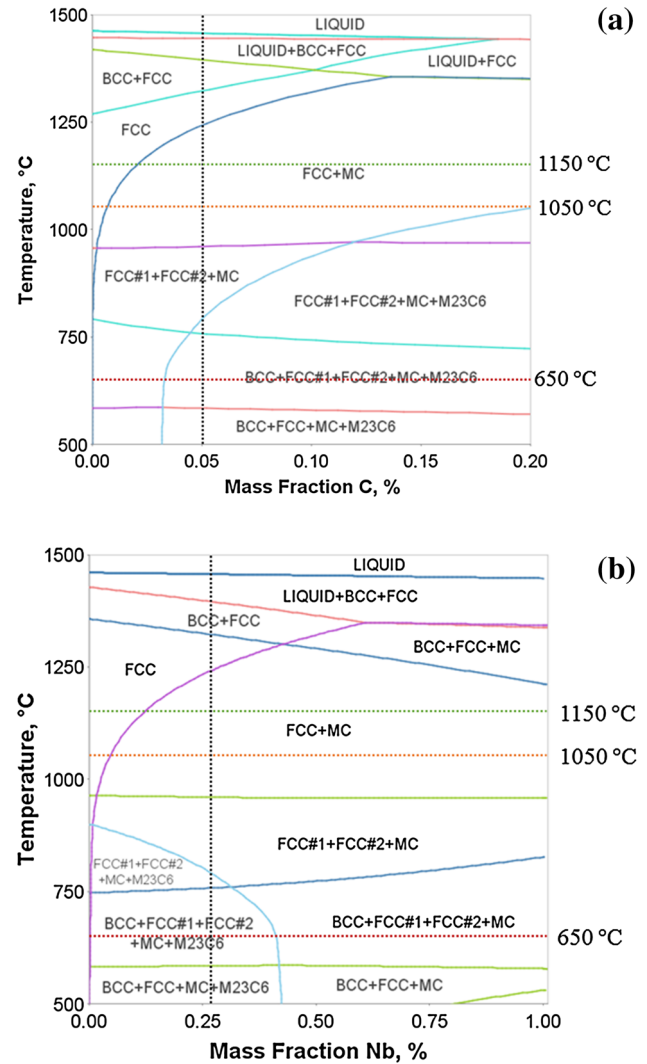


Fig. 8. Isopleth section of the phase diagram for varying mass fractions of (a) C and (b) Nb. Composition of the alloy is indicated by the dotted vertical line while the horizontal dotted lines indicate various temperatures of heat treatment.

(angstrom-sized nano-clusters)² which makes it only resolvable using a transmission electron microscope. At the higher temperature of 1050°C, the mass fraction of carbides is expected to be much less than 1%.

Effect of AMS 5355 Homogenization Heat Treatment

Both macro- and microsegregation are known to occur in cast alloys depending on the solidification rate, composition of the alloy, mode of heat conduction, and size of the casting. For the 17-4 steel cast alloy analog CB7Cu-1, AMS 5355 recommends a homogenization heat treatment at a temperature of 1150°C for > 90 min prior to solutionizing at 1050°C in order to reduce this segregation and achieve a more uniform microstructure and chemistry.²⁰ Due to the similarities of AM 17-4 to cast alloys, (though

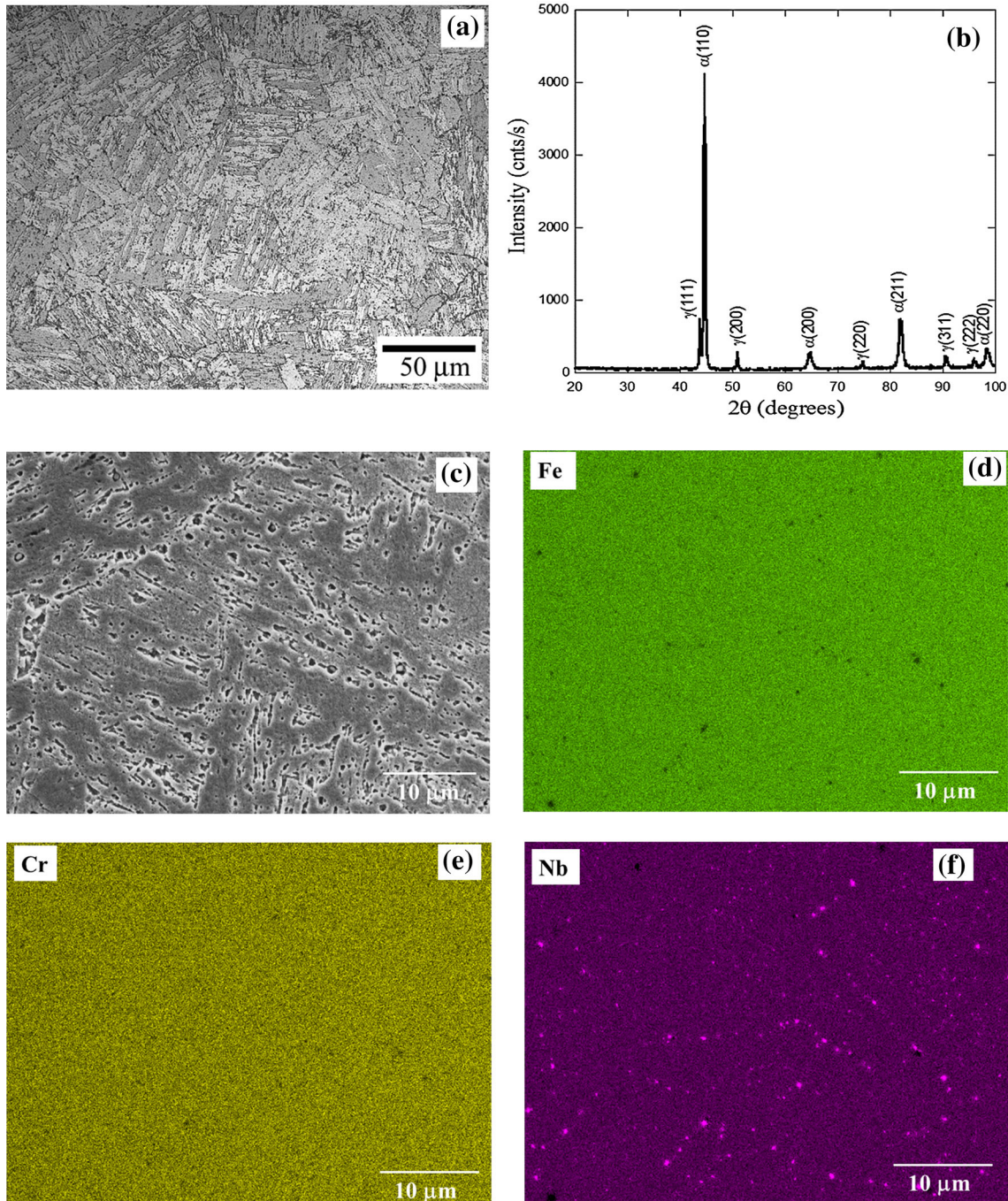


Fig. 9. (a) Optical micrograph, (b) XRD pattern, (c) SE image, (d–f) x-ray maps for Fe, Cr and Nb, respectively, obtained parallel to the build direction from AM-H steel.

thermal cycling and cooling rates are much higher during AM), this cast alloy homogenization heat treatment procedure is employed here on AM 17-4 steel. Figure 9a and b shows the optical micrograph and XRD pattern obtained from AM-H steel. The dominant microstructural constituent is martensite with the amount of retained austenite reduced to $\approx 10\%$. High-magnification SE image (Fig. 9c) and

x-ray maps (Fig. 9d–f) show the complete elimination of microsegregation and the presence of coarsened MC carbides along prior dendrite boundaries (Fig. 9f). Though retained austenite is still present, the AM-H material has a microstructure closest to that observed for conventional wrought material. The hardness (288 ± 32 VHN) is higher compared to AM-AB, but lower than AM-S or wrought steels.

An additional solutionizing treatment at 1050°C for 30 min increased the hardness to be comparable to that of W-S steel, though the relative fraction of γ phase remained the same at about 10%.

The results of the AMS 5355 homogenization heat treatment on AM 17-4 steel demonstrate the utility of post-build thermal processing in creating a more uniform microstructure resembling that of the wrought counterparts. The 10% or so of the remaining retained austenite is likely caused by nitrogen trapped in the solid solution as a result of the powder atomization process and AM build environment, both of which used nitrogen gas, as both the other potential causes of significant retained austenite, a fine subgrain size and enrichment of an austenite stabilizing element in the as-solidified FCC phase, have been eliminated. Ideally, post-build homogenization would be performed above 1250°C where the NbC carbides are dissolved, and in vacuum or nitrogen-poor atmosphere to remove as much nitrogen as possible from the material. However, both processes involve added cost of production and may not be industrially acceptable. Within the more industrially friendly FCC + MC temperature window ($\approx 1050^\circ\text{C}$ to 1250°C), heat treatment in the low-temperature regime may not yield a uniform microstructure due to slower diffusion kinetics, whereas in the high-temperature regime, coarsening of pre-existing carbides may be unavoidable. Hence, it is essential to optimize both temperature and time of homogenization heat treatment for AM 17-4 steel to achieve a fully martensitic structure consisting of fine Nb carbides. Further experiments are currently in progress to identify the most effective heat treatment procedure for industrial applications, study the details of the resulting microstructures, including texture and texture evolution during thermal processing, and to perform a more comprehensive investigation of mechanical behavior of AM 17-4 steel processed via this optimized heat treatment compared to its wrought counterpart.

CONCLUSION

- Additively manufactured 17-4 PH stainless steel exhibited a dendritic/cellular solidification microstructure in the as-built condition.
- The as-built material consisted of roughly equal volume fractions of BCC/martensite and FCC (austenite) phases in contrast to a fully martensitic/BCC structure observed in wrought 17-4 steel.
- Industry-recommended post-build stress relief annealing of AM 17-4 PH steel at 650°C for 1 h was not effective in altering the directionally solidified microstructure, although hardness increased significantly.
- Conventional wrought 17-4 PH solution heat treatment of AM 17-4 steel reduced the volume

fraction of FCC/austenite in the microstructure, but proved insufficient to alleviate the segregation resulting from the solidification process.

- The heat treatment regimen prescribed in AMS 5355 for cast steel alloy CB7Cu-1, particularly the 1150°C homogenization anneal, successfully breaks up the dendritic solidification microstructure and alleviates the microsegregation, producing a microstructure comprised of approximately 90% BCC/martensite, with only 10% FCC/austenite remaining, while also increasing the Vickers microhardness to that expected for conventional wrought 17-4 PH.

ACKNOWLEDGEMENT

The authors would like to thank the NIST Engineering Laboratory for building the additively manufactured 17-4 steel used in this study.

REFERENCES

1. ATI technical data sheet, Stainless steel AL 17-4™ precipitation hardening alloy. <http://www.specialtysteelsupply.com/brochure/17-4-technical-data.pdf>. Accessed 1 Apr 2015.
2. J.-H. Wu and C.K. Lin, *J. Mater. Sci.* 38, 965 (2003).
3. H. Mirzadeh and A. Nazafizadeh, *Mater. Chem. Phys.* 116, 119 (2009).
4. M. Murayama, Y. Katayama, and K. Hono, *Metall. Mater. Trans.* 30A, 345 (1999).
5. U.K. Viswanathan, S. Banerjee, and R. Krishnan, *Mater. Sci. Eng. A* 104, 181 (1988).
6. C.N. Hsiao, C.S. Chioub, and J.R. Yanga, *Mater. Chem. Phys.* 74, 134 (2002).
7. R.M. Mahamood, E.T. Akinlabi, M. Shukla, and S. Pityana, *Lasers Eng.* 27, 161 (2014).
8. L.E. Murr, *Additive Manuf.* 5, 40 (2015).
9. W.E. Luecke and J.A. Slotwinski, *J. Res. Natl. Inst. Stan. Technol.* 119, 398 (2014).
10. I. Tolosa, F. Garcandía, F. Zubiri, F. Zapirain, and A. Esnaola, *Int. J. Adv. Manuf. Technol.* 51, 639 (2010).
11. M. Averyanova, P. Bertrand, and B. Verquin, *Annals of DAAAM for 2010 and Proceedings of the 21st International DAAAM Symposium*, ed. B. Katalinic (Austria: DAAAM International, 2010), 21(1), ISSN 1726-9679, ISBN 978-3-901509-73-5.
12. L.E. Murr, E. Martinez, J. Hernandez, S. Collins, K.N. Amato, S.M. Gaytan, and P.W. Shindo, *J. Mater. Res. Technol.* 1, 167 (2012).
13. L.E. Murr, E. Martinez, K.N. Amato, S.M. Gaytan, J. Hernandez, D.A. Ramirez, P.W. Shindo, F. Medina, and R.B. Wicker, *J. Mater. Res. Technol.* 1, 42 (2012).
14. H. Khalid Rafi, D. Pal, N. Patil, T.L. Starr, and B.E. Stucker, *J. Mater. Eng. Perf.* 23, 4421 (2014).
15. T.L. Starr, H. Khalid Rafi, B.E. Stucker, and C.M. Scherzer, *Proceedings of the 23rd Annual International Solid Free-form Fabrication Symposium* (University of Texas, Austin, 2012), pp. 439–446.
16. Mention of commercial products is provided for completeness and does not imply endorsement by NIST, nor does it imply that such products are necessarily the best available for the purpose.
17. D.D. Gu, W. Meiners, K. Wissenbach, and R. Poprawe, *Int. Mater. Rev.* 57, 133 (2012).
18. EOS Material data sheet, EOS stainless steel GP1 for EOSINT M 270. <http://www.eos.info/material-m>. Accessed 23 Oct 2014.
19. AK Steel product data bulletin, 17-4 PH stainless steel. http://www.aksteel.com/pdf/markets_products/stainless/precipitation/17-4_PH_Data_Bulletin.pdf. Accessed 1 Apr 2015.

20. Aerospace material specification, Steel, corrosion resistant, investment castings 16Cr-4.1Ni-0.28Cb-3.2Cu-homogenization and solution heat treated or homogenization, solution, and precipitation heat treated. <http://standards.sae.org/ams5355/>. Accessed 18 May 2015.
21. Thermo-Calc 3.0, Thermo-Calc Software AB, Stockholm, Sweden, 2013.
22. TCFE6 Fe-based alloy database, Thermo-Calc Software AB, Stockholm, 2009.
23. T. Vilaro, C. Colin, and J.D. Bartout, *Metall. Mater. Trans. A* 42, 3190 (2011).
24. Q. Chen and B. Sundman, *Mater. Trans.* 43, 551 (2002).
25. W. Wu, L.Y. Hwu, D.Y. Lin, and J.L. Lee, *Scripta Mater.* 42, 1071 (2000).
26. R. Colaco and R. Vilar, *Mater. Sci. Eng. A* 385, 123 (2004).
27. K. Kempen, E. Yasa, L. Thijs, J.-P. Kruth, and J. Van Humbeeck, *Phys. Procedia* 12, 255 (2011).
28. R. Colaco and R. Vilar, *J. Mater. Sci. Lett.* 17, 563 (1998).
29. D. Das, A.K. Dutta, and K.K. Ray, *Mater. Sci. Eng. A* 527, 2182 (2010).